Purdue University

Purdue e-Pubs

CTRC Research Publications   Cooling Technologies Research Center

2021

Topology Optimization of Microchannel Heat Sinks using a Homogenization Approach

S. Ozguc
Purdue University

L. Pan
Purdue University

J. A. Weibel
Purdue University, jaweibel@purdue.edu

Follow this and additional works at: https://docs.lib.purdue.edu/coolingpubs

Ozguc, S.; Pan, L.; and Weibel, J. A., "Topology Optimization of Microchannel Heat Sinks using a Homogenization Approach" (2021). *CTRC Research Publications.* Paper 372.
http://dx.doi.org/https://doi.org/10.1016/j.ijheatmasstransfer.2020.120896

Topology Optimization of Microchannel Heat Sinks using a Homogenization Approach

Serdar Ozguc, Liang Pan, Justin A. Weibel

Cooling Technologies Research Center and School of Mechanical Engineering

Purdue University, 585 Purdue Mall, West Lafayette IN 47907

Abstract

Topology optimization for heat sink devices typically relies on penalization methods to ensure the final designs are composed of strictly solid or open regions. In this work, we formulate a homogenization approach wherein the partial densities are physically represented as porous microstructures. This formulation allows design of thermal management components that have sub-grid features and leverages additive manufacturing techniques that can produce such partially porous regions within the build volume. Topology optimization of a liquid-cooled microchannel heat sink is presented for a hotspot over a uniform background heat input. The partial densities are represented as arrays of pin fins with varying gap sizes to achieve sub-grid-resolution features. To this end, the pin fins are modeled as a porous medium with volume-averaged effective properties. Height-averaged two-dimensional flow and non-equilibrium thermal models for porous media are developed for transport in the pin fin array. Through multi-objective optimization, the hydraulic and the thermal performance of the topologically optimized designs is investigated. The pin fin geometry is bounded based on the capabilities of state-of-the-art direct metal laser sintering machines. The resulting topologies have porous-membrane-like designs where the liquid is transported through a fractal network of open, low-hydraulic–resistance manifold pathways and then forced across tightly spaced arrays of pin fins for effective heat transfer. The effects of the grid resolution and the initial design guess on the resulting topologies and performances are reported. The topologically optimized designs are revealed to offer significant performance improvements relative to the benchmark, a straight microchannel heat sink with features optimized under the same multi-objective cost function. The work demonstrates that representing partial densities as porous microstructures results in resolution-independent performance at much smaller grid sizes through the use of sub-grid

features compared to topology optimization methods that incorporate penalization methods for strictly solid and open designs.

Keywords

topology optimization, additive manufacturing, microchannel heat sink, multi-objective optimization, hotspot

Nomenclature

c	coolant specific heat capacity, J/kg-K
D_h	hydraulic diameter, m
f	friction factor, -
f_{obj}	objective function, -
h	convection coefficient, W/m²-K
h_b	base effective heat transfer coefficient, W/m²-K
H_b	base thickness, m
h_f	coolant effective heat transfer coefficient, W/m²-K
h_s	solid fin effective heat transfer coefficient, W/m²-K
H_t	channel/microstructure height, m
K	flow permeability, m²
$K_{c,e}$	height-averaged energy equation coefficient, -
$K_{c,m}$	height-averaged momentum equation coefficient, -
$K_{d,m}$	height-averaged viscous shear coefficient -
k_f	coolant thermal conductivity, W/m-K
k_s	thermal conductivity of the solid, W/m-K
$k_{s,xy}$	effective in-plane thermal conductivity of the microstructure, W/m-K
$k_{s,z}$	effective vertical thermal conductivity of the microstructure, W/m-K
n	number of grid cells, -
Nu	Nusselt number, -
ΔP	overall pressure drop, Pa
ΔP_u	utopian pressure drop, Pa
Q_{in}	net heat input, W
$Q_s^{''}$	heat flux at the heat sink bottom surface, W/m²

R_p pseudo thermal resistance, K/W

R_{max} thermal resistance based on maximum temperature, K/W

R_u utopian thermal resistance, K/W

Re Reynolds number, -

T_b base temperature, K

t_f fin thickness, m

T_f coolant temperature, K

T_{in} inlet coolant temperature, K

T_s microstructure temperature, K

v velocity vector, m/s

w_c channel width, m

Greek Symbols

α multi-objective weighting coefficient, -

ε_i design variable

μ coolant dynamic viscosity, Pa-s

ρ coolant density, kg/m^3

ρ_A specific surface area, 1/m

1. Introduction

The demand for miniaturization of electronic devices calls for novel thermal management solutions that can extract high heat loads from compact spaces. Additive manufacturing (AM) enables the fabrication of complex heat transfer geometries with high performance and may eliminate thermal interface resistances by fabricating multi-component cooling systems as single parts. Metal AM technologies such as direct metal laser sintering (DMLS) and selective laser melting (SLM) create new avenues for designing high-performance thermal management solutions due to the availability of high thermal conductivity metals for 3D printing.

Various novel heat sink designs have been proposed to utilize the design freedom brought by metal AM. Wong et al. [1] fabricated three novel heat sink designs using SLM in aluminum 6061, demonstrating the capability of producing parts with complex features that would be challenging to manufacture using conventional methods. Fasano et al. [2] designed and

fabricated a pitot tube heat sink incorporating secondary flow patterns orthogonal to the main flow for enhanced heat transfer in stagnant regions and reported a 98% improvement in heat transfer performance relative to their conventional benchmark design. Tseng et al. [3] used body-centered cubic lattice structures to generate several novel heat sink designs which were 3D printed in a titanium alloy. The geometric parameters defining the lattice structures were locally varied within the novel designs to increase the flow rate near the bottom surface and also to enhance the fin efficiency using thicker fins near regions of high heat transfer. Testing demonstrated that the design with a non-uniform lattice offered a 26% reduction in thermal resistance compared to the homogeneous design. Ozguc et al. [4] used DMLS to 3D print a vapor chamber, fabricated as a single piece that could be embedded within 3D printed heat sink designs for enhanced heat spreading with no interfacial resistances. Collins et al. [5] proposed a permeable membrane microchannel (PMM) heat sink design which incorporated wavy, porous membranes with fine internal flow features for effective heat dissipation to the coolant at low pressure drop. The PMM heat sink was fabricated using DMLS in AlSi10Mg and the wavy porous structure was achieved through partial sintering of the metal powder with adjusted laser parameters; enhanced performance over the benchmark manifold microchannel heat sink was demonstrated. Ozguc et al. [6] performed a parametric optimization of the PMM design and reported reduced thermal resistance relative to an optimized conventional microchannel heat sink design under conditions where maintaining a low pressure drop is prioritized. A PMM design was fabricated using DMLS in AlSi10Mg and X-ray microtomography of the part showed that optimal channel sizes on the order of ~10s of microns were successfully fabricated.

Proposed novel AM heat sink designs have generally been shown to outperform their conventional counterparts. Even though they show great promise, these intuition-based designs might fail to leverage the full potential of the design freedom brought by AM, especially for design scenarios having complex boundary conditions and multiple competing performance objectives. There is a need to explore the AM design space using autonomous design algorithms requiring minimum user-input. Topology optimization is a mathematical method that optimizes the material distribution within a design space for a given objective function. Topology optimization is known to result in high-performance parts, but with complex geometries that are often so difficult to manufacture using conventional methods that the increased fabrication cost

is not justified. On the other hand, the cost of most AM processes is independent of part complexity, making these processes well-suited for fabrication of topologically optimized designs. Topology optimization can generate high-performance heat sinks, and AM can fabricate these more complex parts with no additional cost.

Topology optimization has been commonly used for structural mechanics applications, and has also been applied to many other fields, as reviewed in detail elsewhere [7, 8]. Of specific interest for the current study is the use of topology optimization to address multi-physics thermal management problems. Koga et al. [9] developed water-cooled, low-velocity heat sinks designed by topology optimization using the Stokes flow approximation. Zhao et al. [10] used topology optimization to produce fins for thermal energy storage systems and reported a lower-weight, material-saving design in comparison to several conventional fin geometries. Zeng et al. [11] generated an air-cooled heat sink design using topology optimization and experimentally demonstrated a reduced junction temperature at a given pumping power relative to a straight channel design. Dede [12] topologically optimized jet impingement surfaces for reduced device temperatures. Although most thermal management components have three-dimensional transport characteristics, these prior studies have typically used approximate two-dimensional multi-physics models due to the high computational overhead costs accompanied by topology optimization algorithms. Three dimensionality has been included in some studies through simplified models, parallel computing, and with large computational resources. Dede [13] designed a multi-layer branching microchannel heat sink by combining multiple topologically optimized 2D designs with matched boundary conditions. Alexandersen et al. [14] performed a 3D topology optimization of heat sinks cooled with natural convection using the Bousinessq approximation to simplify the buoyancy-driven flow and a parallel computation framework to solve the resulting large scale non-linear multiphysics problem. Dilgen et al. [15] performed a 3D topology optimization of heat sinks with turbulent forced convection and highlighted the benefits of using full 3D optimization and including turbulence modeling. AM has been leveraged in some topology optimization studies with the acknowledgement of its ability to fabricate the resulting complex geometries. Dede et al. [16] generated a topologically optimized air-cooled heat sink, fabricated the design using AM out of AlSi12, and experimentally showed an improved coefficient of performance relative to the conventionally manufactured plate and

pin fin heat sinks. Lazarov et al. [17] used AM to fabricate a topologically optimized natural convection heat sink for thermal management of light-emitting-diode lamps. Experimental characterization of the 3D-printed heat sink showed 21-23% lower temperature using 17% less material relative to the benchmark solution.

In topology optimization there are several approaches to optimize the material distribution within a design space as discussed by Haber and Bendsoe [18]. In most of the approaches, the design space is discretized, and the material distribution is represented by a characteristic function that varies within the design space between values of 0 and 1 (where 1 represents the solid phase and 0 represents the void/liquid phase). Most of the prior topology optimization studies in thermal management of electronic devices have used the 'restricted' problem formulation. In the restricted formulation, the partial densities represented by this formulation hold no physical meaning and are a means to avoid an ill-posed optimization problem. In these cases, the restricted formulation uses penalization algorithms to strictly penalize inclusion of partial densities within the design space so as to achieve admissible designs that consists of only 0 or 1. On the other hand, the 'relaxed' problem formulation represents the partial densities using microstructures having characteristic properties that can be defined with known analytical functions, as discussed by Bendsoe and Sigmund [19]. This approach has been primarily avoided due to the cost and complexity of manufacturing such microstructure using conventional manufacturing methods.

Formulation of the partial densities in topology optimization as microstructures of varying properties has several potential benefits versus using penalization approaches. Penalization of the partial densities has the purpose of improving manufacturability at the drawback of non-optimal performance. Therefore, the relaxed formulation has been suggested by Haber and Bendsoe [18] for determination of physical limits on the achievable performance, provided that incorporation of partial densities is possible. With high-resolution AM technologies available, partial densities can be realized as microstructures and higher performance parts can potentially be achieved. Additionally, the discretization of the design space in topology optimization is often limited by high computational costs. Representing partial densities as porous microstructures allows designs to incorporate sub-resolution features that would be computationally expensive to capture using

conventional topology optimization. Lastly, implementation of the partial densities allows for multi-scale topology optimization where the formulation of the microstructures can be achieved through a separate optimization problem. For example, Zhu et al [20] generated a bulk material property dataset using multi-material microstructures and performance multi-scale structural mechanics topology optimization using these microstructures as the building blocks within the design space. Some of the resulting geometries were fabricated using multi-material 3D printing.

Topology optimization and additive manufacturing have been explored for design of thermal management devices, with a few studies that specifically investigate liquid-cooled microchannel heat sinks; formulation of the partial densities as 3D printable porous microstructures has not yet been investigated. In this paper, a topology optimization algorithm is formulated using a homogenization approach for the design of microchannel heat sinks, incorporating microstructures (namely, pin fin arrays) that are suitable for 3D printing to physically represent partial densities in the design domain. A multi-objective optimization approach is used to investigate the resulting designs, for a hotspot over a uniform background heat input, which are then compared to optimized conventional designs for performance evaluation. The liquid flow fields and temperature maps of the resulting designs are discussed, and the effects of certain hyperparameters used in the optimization process are studied.

2. Methodology

In the design of microchannel heat sinks (MCHS), the hydraulic (overall pressure drop) and thermal (thermal resistance) performance are of interest, often captured by some single performance metric that accounts for both. In this study, a multi-objective optimization approach is implemented to investigate the trade-off between these two aspects of performance. The weighted sum approach is used to formulate the multi-objective optimization problem as follows:

$$\text{minimize } f_{obj}(\varepsilon_i) = \alpha \frac{\Delta P(\varepsilon_i) - \Delta P_u}{\Delta P_u} + (1-\alpha) \frac{R_p(\varepsilon_i) - R_u}{R_u} \qquad [1]$$

$$\text{where } 0 \leq \varepsilon_i \leq 1$$

To represent the material distribution, the design space is discretized into cells and a design variable ε_i is assigned to each cell to represent the so-called 'density' (i.e., porosity) of the material within the cell. With the implementation of the partial densities as microstructures, the design variables do not need to correspond to the densities/porosities within the cells but can be used to model the physical dimensions of the microstructures. The terms $\Delta P(\varepsilon_i)$ and $R_p(\varepsilon_i)$ in Equation 1 are the overall pressure drop and the thermal resistance of the design defined by the set of design variables ε_i, respectively. The terms ΔP_u and R_u are the utopia points used for scaling purposes and do not affect the results. The term n is the user-defined weighting coefficient that controls the importance given to each objective during optimization.

Fluid flow and heat sink temperature information are needed for a given MCHS design to evaluate the objective function. Approximate 2D models are often preferred over 3D models to counter the high-computational costs associated with the iterative nature of topology optimization. However, transport in MCHS designs involves 3D effects that are crucial to the performance of the device. Presence of a velocity profile along the channel height due to the bottom and top surfaces increases the viscous shear on the flow. Temperature profiles along the fins and within the coolant affect the convective heat transfer performance. Lastly, the solid base of a MCHS spreads the heat from hotspots into the fins, which cannot be captured using a purely 2D model. Van Oevelen [21] averaged the 3D mass, momentum, and energy conservation equations over the height of the domain to obtain 2D conservation equations. Velocity and temperature profiles along the height are assumed to perform the averaging operation. The resulting 2D model accounts for diffusive momentum and energy transport along the height of the domain. An additional averaging operation is done on the bottom solid layer of the MCHS domain in order to capture heat spreading in the base. The same height-averaging approach has been adopted in this study for conservation of mass and momentum, and readers are referred to Ref. [21] for more details on the derivation. The resulting governing 2D mass and momentum transport equations respectively are:

$$\nabla \cdot v = 0 \tag{2}$$

$$K_{c,m}\nabla \cdot \rho v v - \nabla \cdot \mu \nabla v + \nabla P + \mu \left(\frac{K_{d,m}}{H_t^2} + \frac{1}{K(\varepsilon_i)} \right) v = 0 \tag{3}$$

For the governing energy transport equations Van Oevelen [21] used a local thermal equilibrium model where the solid and the liquid within a partially dense unit cell were assumed to have the same temperature. Because these partial densities were penalized and the final designs consisted of distinct solid and liquid regions, this local temperature equilibrium assumption was inconsequential. However, in this study, penalization algorithms are not used and the partial densities are implemented as microstructures. Therefore, the height-averaging operation has been reformulated for a local thermal non-equilibrium model. Adoption of a non-equilibrium model introduces an additional energy conservation equation for the second phase within the unit cells and the resulting governing 2D energy equations within the solid microstructure, the liquid, and the solid base respectively are

$$-H_t \nabla \cdot k_s(\varepsilon_i) \, \nabla T_s - H_t \rho_A(\varepsilon_i) h(\varepsilon_i) \left[T_s - T_f \right] + \frac{h_b h_s(\varepsilon_i)}{\sum h_k(\varepsilon_i)} (T_s - T_b) + \frac{h_s(\varepsilon_i) h_f}{\sum h_k(\varepsilon_i)} (T_s - T_f) = 0 \qquad [4]$$

$$K_{c,e} H_t \nabla \cdot \rho c v T_f - H_t \nabla \cdot k_f(\varepsilon_i) \, \nabla T_f - H_t \rho_A(\varepsilon_i) h(\varepsilon_i) \left[T_f - T_s \right] + \frac{h_b h_f}{\sum h_k(\varepsilon_i)} (T_f - T_b) + \frac{h_s(\varepsilon_i) h_f}{\sum h_k(\varepsilon_i)} (T_f - T_s) = 0 \qquad [5]$$

$$-H_b \nabla \cdot k_b \nabla T_b - Q_s'' - \frac{h_b h_s(\varepsilon_i)}{\sum h_k(\varepsilon_i)} (T_s - T_b) - \frac{h_s(\varepsilon_i) h_f}{\sum h_k(\varepsilon_i)} (T_f - T_b) = 0 \qquad [6]$$

In the governing equations above: $K_{c,e}$ is a constant that accounts for the effects of a velocity profile along the height on energy transport; and h_b, h_s, and h_f account for the effects of a temperature profile along the height on heat diffusion. These terms are calculated using the averaging operation after assuming velocity and temperature profiles along the height as described in Ref [21]. A hydrodynamically and thermally fully developed velocity profile between parallel plates was assumed for the fluid. A linear temperature drop was assumed across the heat sink base. Distinct from Ref. [21], the temperature profile along the microstructure height was determined by using the standard fin analysis which assumes a uniform temperature at any given cross-section along the fin height and a uniform convection coefficient at the solid-liquid interface.

The governing partial differential equations are discretized using the finite volume method. The discretized conservation of mass and momentum equations are solved using the semi-implicit

method for pressure linked equations (SIMPLE) algorithm with the first-order upwind scheme. The discretized energy equations resulted in a set of linear equations which are solved using matrix inversion. The 2D model is implemented in MATLAB and solved for velocity, pressure, and temperature fields for a MCHS design represented by the material distribution. The overall pressure drop is calculated as the average pressure difference between the inlet and the fixed pressure at the outlet. In thermal management applications, the limiting factor is often the maximum local temperature of the heat-generating surface instead of the average. However, using the absolute maximum temperature as an objective poses an ill-conditioned optimization problem because the highest-temperature point shifts within the design space during iteration of the material distribution. Therefore, an optimizer-friendly pseudo thermal resistance is used in the objective function, defined as

$$R_p(\varepsilon_i)= \frac{1}{Q_{in}}\left[\frac{1}{n}\sum\left(T_{b,i}(\varepsilon_i)-T_{in}\right)^m\right]^{\frac{1}{m}} \tag{7}$$

In this pseudo thermal resistance, the difference between the local heat sink base temperature and the coolant temperature at the inlet is taken to the power m before averaging over the design space. The value of m is chosen so that the points with higher temperatures in the design space have more weight on the performance. A value of $m=10$ was found to give designs with low maximum temperature and still have good convergence. Nevertheless, the thermal resistance defined based on the absolute maximum temperature in the design space defined is used for the evaluation of the thermal performance after the optimization is completed.

$$R_{max}(\varepsilon_i)=\frac{max\left[T_{b,i}(\varepsilon_i)\right]-T_{in}}{Q_{in}} \tag{8}$$

The method of moving asymptotes (MMA) by Svanberg [22] commonly used in topology optimization problems is implemented in this study. In MMA, a convex approximating subproblem is solved at each design iteration and the asymptotes of the subproblem are updated based on the stability of the design variables. MMA uses gradient information which is calculated at each iteration using the adjoint state method. The resulting sensitivities are filtered

using the filtering scheme described by Sigmund [23] to avoid checkerboard patterns. Convergence is assumed when a design stops changing between consecutive iterations.

In the restricted approach to topology optimization, partial densities used only for optimization purposes do not hold a physical meaning. Therefore, various interpolation approaches have been used to model the faux properties associated with these partial densities with the intent to avoid an ill-conditioned optimization problem. In this study, partial densities are represented as microstructures having variable effective properties for which analytical expressions are needed to solve the design problem. Additionally, the choice of microstructure should be within the capabilities of current metal AM technologies to generate manufacturable designs. Direct metal laser sintering (DMLS) has been chosen as the reference metal AM technology due to its technoeconomic advantages discussed by Collins et al. [24]. In our recent work [6], DMLS was used to fabricate AlSi10Mg pin fin arrays for liquid cooling applications with a minimum solid fin thickness of 150 µm and tight spacings. Therefore, AlSi10Mg square pin fin arrays with an in-line configuration are chosen in this study as the microstructure to represent the partial densities. Although the performance of the pins of such small feature sizes can be significantly altered by the high surface roughness associated with metal additive manufacturing processes as demonstrated in Ref. [6], a smooth wall assumption is used for simplicity in this paper. Figure 1 defines the pin fin array geometry and dimensions, can be described using only two variables: the fin thickness (t_f) and the channel width (w_c). A constant fin thickness of 150 µm is used throughout this study and the channel width is allowed to vary to capture the design variable range between 0 and 1 as

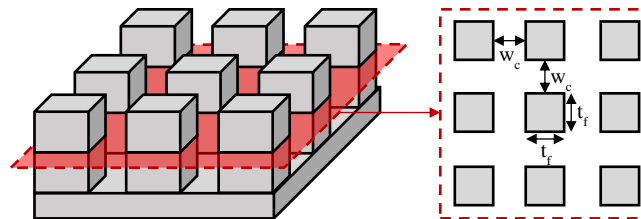$$\varepsilon_i = \frac{w_c}{t_f + w_c}$$

[9]

Figure 1: Schematic representation and dimensions of the square pin fin arrays used to represent the partial densities during topology optimization.

Correlations for friction factor and Nusselt number for flow through pin fins are only available for sparsely spaced arrays. Preliminary investigation revealed that the optimization algorithm prefers tightly packed pin fin arrays for which these correlations are not valid. The velocity and temperature profiles for flow through tightly packed pin fins is assumed to be not significantly disrupted by the transverse gap, and therefore would follow a similar behavior as flow between parallel plates. Further, although pin fins do not have an isotropic geometry, properties are assumed to be isotropic for simplicity. The hydraulic diameter for the flow through the pin fins is defined as:

$$D_h(\varepsilon_i) = 2 \cdot w_c(\varepsilon_i) \tag{10}$$

Friction factor and Nusselt number correlations for fully developed flow between parallel plates from Incropera et al. [25] are used, yielding the expressions for flow permeability, heat transfer coefficient, and specific surface area as:

$$K(\varepsilon_i) = \frac{8 \cdot (w_c(\varepsilon_i))^3}{(t_f + w_c(\varepsilon_i))(f \cdot Re)} \text{ where } (f \cdot Re) = 96 \tag{11}$$

$$h(\varepsilon_i) = \frac{Nu \cdot k_f}{2 \cdot w_c(\varepsilon_i)} \text{ where } Nu = 7.54 \tag{12}$$

$$\rho_A(\varepsilon_i) = \frac{2 \cdot t_f}{\left(t_f + w_c(\varepsilon_i)\right)^2} \tag{13}$$

The effective thermal conductivity is calculated based on the geometry and material conductivity k_s of 110 W/m-K for AlSi10Mg [26].

$$k_{s,xy} = 0, \ k_{s,z} = k_s \times \frac{t_f^2}{\left(t_f + w_c\right)^2} \tag{14}$$

A 48/52 water/ethylene glycol mixture is chosen as the coolant with the properties given in Table 1. The topologically optimized designs are compared to a straight microchannel (SMC) heat sink benchmark design for performance evaluation. The SMC heat sink has uniform straight fins and channels that are modeled by modifying the effective properties shown in Equations 10-13 for parallel plates and solving the governing equations with a uniform material distribution. The SMC design is also optimized using the multi-objective optimization approach shown in Equation 1, however, it consists of only two design variables: the channel width and the fin thickness. The interior-point algorithm implemented in MATLAB is used for the optimization of the benchmark.

Table 1: Coolant properties [27].

Coolant	48/52 Water/Ethylene
Viscosity (Pa·s)	3.72×10^{-3}
Density (kg/m^3)	1076
Thermal Conductivity (W/m·K)	0.400
Specific Heat (kJ/kg·K)	3.30

3. Results

The boundary and operating conditions used in this study are shown in Figure 2. A uniform heat flux of 0.45 W/mm^2 is applied over a 15×15 mm^2 area. There is a 1.5×1.5 mm^2 hotspot located within the design space with a heat flux of 4.5 W/mm^2. The design space in which the material distribution is optimized is defined as the same 15×15 mm^2 area, representative of a microchannel heat sink placed directly over a heat-generating surface. The total thickness of the design space is 1.5 mm including the 0.5 mm solid base thickness. The 48/52 water/ethylene glycol mixture enters the design space from the left boundary with a uniformly distributed total flow rate of 200 mL/min and leaves from the right boundary to a uniform reference pressure. In an application, a microchannel heat sink would have an upstream header where the flow would redistribute before entering the heat sink to follow the path of least resistance. This can have a significant impact on the flow and thermal performance and therefore a 3-mm long inlet header is added upstream of the design space. Both the 15×15 mm^2 design space and the 3×15 mm^2

header are discretized for solving the flow and heat transfer, but only the cells within the design space are cast as design variables for topology optimization.
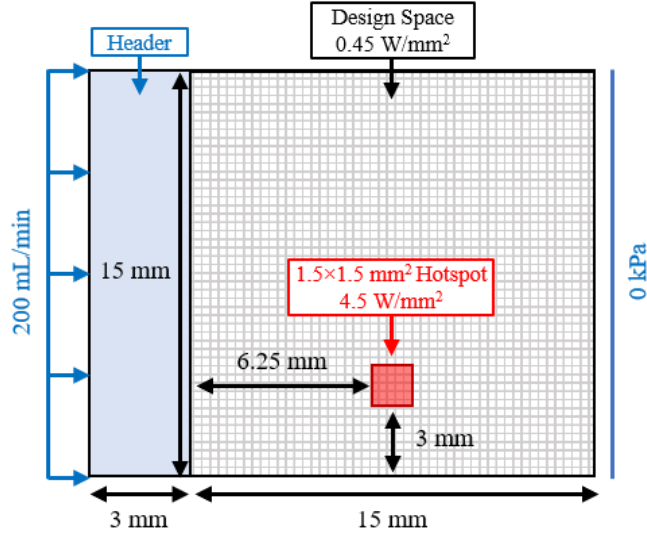

Figure 2: Boundary conditions and dimensions of the design space used for topology optimization of the microchannel heat sink.

The MMA is an iterative optimization algorithm where gradient information is used at each iteration to update the design until convergence. A uniform material distribution of $\varepsilon_i^0 = 0.5$ is given as the initial guess. The multi-objective cost function (Equation 1) uses a weighted sum approach with a user-defined weighting coefficient α. Initially, a weighting coefficient of $\alpha = 0.035$ is used. The design space is discretized in 80×80 cells with a cell size of 187.5 µm (the hotspot is represented by 8×8 cells). A sensitivity filtering radius of 375 µm is found to give checkerboard-pattern-free designs and is used throughout this study. Figure 3 shows the evolution of the material distribution in the design space with iterations. The shades of grey represent the local magnitude of the design variable defined in Equation 9 and the local hotspot is indicated by the translucent red square. The optimizer starts with a uniform shade of gray, ε_i^0. Within the first 20 iterations, large features are created as indicated by the distinct regions of light and dark gray, and the objective function value is sharply decreasing. Between iterations 20 and 50, light grey regions have turned into large, open channels with $\varepsilon_i = 1$ and smaller channels have started to branch out from these open channels into the dark grey. By iteration 50, most of the features in the final optimized topology have formed and the objective function has reduced

significantly compared to the initial guess. The following 150 iterations finely tune the material distribution with minimal further reduction in the objective function as the optimizer fully converges.
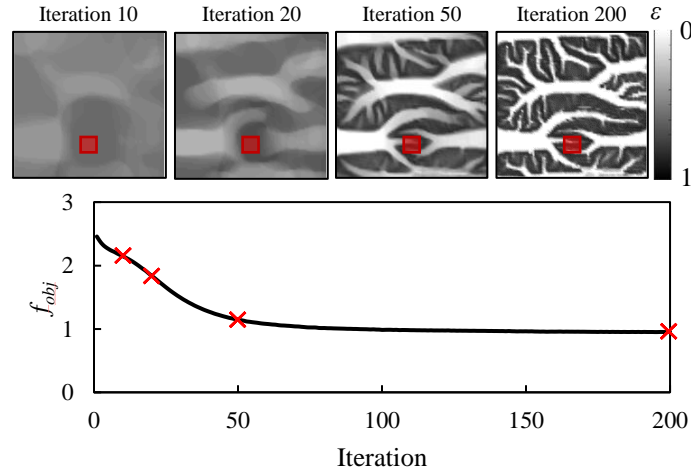

Figure 3: Evolution of the design objective function with number of iterations during topology optimization (80×80 cells; $\varepsilon_i^0 = 0.5$; $n = 0.035$). Grayscale contour maps of the design variable, ε_i, called out along the curve show the material distribution in the design space (hotspot location is indicated by a translucent red overlay)

The final design shown in Figure 4 (a) consists of large white regions separated by dark gray bands, with some fingering of smaller-scale white regions into these dark gray bands. The white regions correspond to $\varepsilon_i = 1$, where the gap between the pin fins becomes so large that it is effectively flow over a flat plate without any pin features. The dark gray regions are pin fin arrays of varying gap sizes represented by the magnitudes of the design variables ε_i. For this particular design, the magnitude of the design variables within the grey regions have a median of 0.27 with lower and upper quartiles of 0.21 and 0.53. This translates to gaps between the 150 µm square pin fins having a median of 50.6 µm with lower and upper quartiles of 39.4 µm and 99.4 µm. Figure 4 (b) shows the flow streamlines through the optimized design. The flow is guided into the large open channels from the inlet header. However, in this particular design, there are no direct routes for flow from the inlet to the outlet through these large channels. Rather, these channels act as internal flow distributors: the coolant enters into an open channel from the left-side inlet, travels deep into the heat sink through an open channel, is forced across a dense pin fin

array, and is then recollected into another open channel from which it can leave the heat sink. Similar flow paths are seen throughout the heat sink regardless of the entry point. Additionally, the resulting topology guides a significant portion of the flow toward the vicinity of the hotspot, via the formation of a large converging channel directly upstream, in an effort to cool it. Figure 4 (c) shows the resulting coolant temperature map. The flow temperature does not increase significantly as it travels through the open channels, but rather there is a large temperature gradient as the coolant is pushed through the pin fins. In fact, the temperature gradient is large enough that the topology of the design, as well as the distinction between inlet and outlet flow channels, can be easily inferred from the temperature map. This indicates that the majority of the heat dissipation occurs as the coolant flows through the pin fins.

The optimizer decided to dedicate a significant portion of the design space for flow through large, open channels even they do not contribute significantly to the heat transfer compared to the pin fin arrays. This is attributed to the low hydraulic resistance associated with the open channels. Conversely, pin fin arrays have improved heat transfer effectiveness but high flow resistance. The optimizer created a fractal-like design where the liquid is routed to the effective heat transfer features through low-hydraulic-resistance pathways. This is similar to the design philosophy of multi-layer manifold microchannel heat sinks [28] that use large manifold channels in a top layer to transport coolant to small microchannels at a bottom layer, for an overall reduction in pressure drop compared to SMC heat sinks, while maintaining the enhanced heat transfer characteristic of microchannel. The design shown in Figure 4 essentially creates such manifold channels within the same single layer as the microscale heat exchange features. The resulting flow structure is remarkably similar in principle to the heat sink design concept proposed by Collins et al. [3], referred to as a permeable membrane microchannel (PMM) microchannel heat sink.
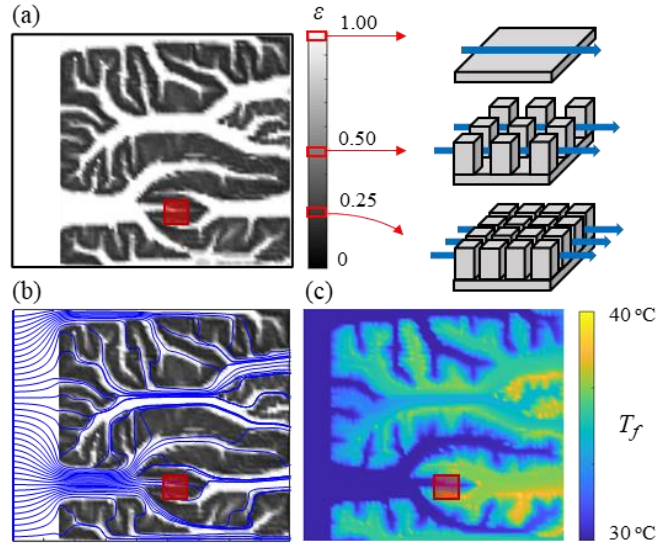
Figure 4: (a) Topologically optimized design from Figure 3 with the schematic images of the microstructure for three different values of the design variable, ε_i, (b) streamlines from the uniform flow velocity inlet to the uniform pressure outlet for the, (c) temperature map of the coolant as it enters from the inlet at 30 °C and flows through the heat sink.

1. *Effect of Design Space Resolution*

A grid resolution of 80×80 was used for the design space in the previous case (Figure 4). The resolution in topology optimization is generally expected to have some effect on the resulting design because a higher resolution would allow for more, finer features to form. Van Oevelen [21] performed topology optimization of microchannel heat sinks over a 10×10 mm² area discretized into 100×100 grid cells using the restricted problem formulation. The resulting designs had multiple one-cell-wide channels as the optimizer was unable to create features smaller than the grid size of 100 μm. However, our previous work [6] has shown that optimized microchannel heat sink designs can consist of channels on the order of 10s of microns. To understand the effect of resolution for the relaxed problem formulation, the grid size is changed while keeping all the parameters consistent, and the resulting designs and their performance are investigated. The pin fin thickness is kept constant at 150 μm and the distance between the pin fins is varied through the design variable, ε_i, as shown in Equation 9. Therefore, a single value for the design variable represents the microstructure with the same dimensions irrespective of the grid resolution. Figure 5 shows the resulting thermal resistances and pressure drops for

topologically optimized designs at four different grid resolutions. At a very coarse resolution of 20×20, the performance is noticeably worse, yielding a design with a higher pressure drop and thermal resistance compared to the highest 80×80 resolution . However, at resolutions of 40×40 and 60×60, the resulting topology captures the same macroscale features as 80×80. Even though some of the finest features are not resolved at these intermediate resolutions, both the hydraulic and the thermal performance are very similar to the highest resolution. It is interesting to note that the performance of the design converges at such a low resolution for topology optimization, where even the very coarse resolution does not have a significant performance penalty. In the current topology optimization approach, where each cell is modeled using a physical microstructure, the optimizer has the ability to use sub-resolution features within the design space. This eliminates the need to use very high resolutions that would be computationally expensive. The smallest feature captured by the design shown in Figure 4 using a 40×40 resolution is a pin fin gap of 26.5 µm ($\varepsilon_i = 0.15$). The restricted problem formulation would need a resolution of 567×567 to resolve a feature of the same size, a two hundred-time increase in the number of grid cells. We note that these results are specific to the case and different boundary conditions (e.g., the hotspot size), but generally expect that the performance would become resolution-independent at much smaller grid sizes using the current relaxed problem formulation compared to the restricted approach. A resolution of 60×60 is used for the rest of this study.
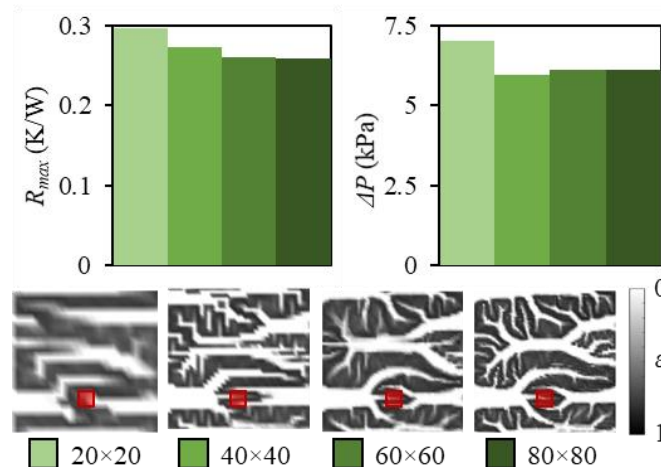

Figure 5: Grayscale contour maps of the topologically optimized designs generated for the same design space (Figure 2) using four different grid resolutions and bar charts showing the resulting thermal resistance and pressure drop values for each design.

All of the design optimization cases presented above were obtained using an initial uniform material distribution guess of $\varepsilon_i^0 = 0.5$. Like most topology optimization cases, the studied problem is expected to have many local minima, and therefore the initial guess dictates which minima the optimizer will converge to. To investigate the effect of the initial guess on the design, and concomitantly the performance, the optimizer was run at different initial designs and the results are summarized in Figure 6. A weighting coefficient of $\alpha = 0.035$ was used. The optimized topologies, as indicated by the material distribution contours, have significantly different appearances for different initial designs. Although the specific topologies differ, the same characteristic flow features appear in all of the designs (viz., open manifold inlet/outlet channels feeding dense pin field arrays). Accordingly, the difference in the performance of the designs is minor. Therefore, we conclude the resulting performance is practically independent of the initial guess when a uniform material distribution is used for the given case. A similar independence of the performance on the initial design guesses was also observed when investigating the case for different weighting coefficients and grid resolutions.
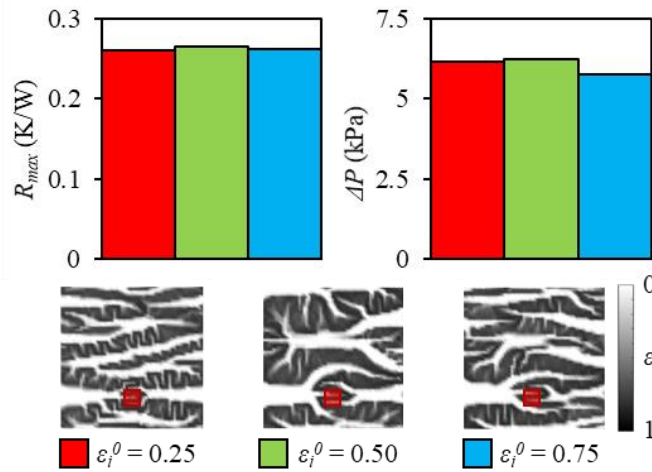

Figure 6: Grayscale contour maps of the topologically optimized designs generated for the same design space (Figure 2) using different initial uniform material distributions, ε_i^0, and bar charts showing the resulting thermal resistance and pressure drop values for each design.

The weighting coefficient of $\alpha = 0.035$ has been used in the previous cases for the multi-objective cost function (Equation 1). This user-defined constant represents the relative importance given to the two objectives used in the cost function, namely, pressure drop versus

thermal resistance. Performance of the topologically optimized designs is investigated using a pareto optimality approach in which the optimizer is run using different weighting coefficients. The resulting pareto optimality curve shows the trade-off between the two objectives, pressure drop and thermal resistance, and can be seen in Figure 7. Thermal resistance and pressure drop of the topologically optimized designs at different weighting coefficients are represented on the pareto optimality curve by the abscissa and ordinate, respectively. As the weighting coefficient is decreased, more priority is given to the thermal performance. As a result, more of the design space becomes covered with pin fins of tight spacing rather than the large open channels (as indicated by a darkening of the material distribution contours). As a consequence, the thermal resistance is reduced due to enhanced heat transfer within the pin fins at the expense of increased pressure drop. Conversely, as the weighting coefficient is increased and more weight is given to the hydraulic performance, open channels enlarge and reduce the overall pressure drop at the expense of increased thermal resistance. At the extreme high-weighting-coefficient end of the resulting pareto optimality curve, there are designs with large open channels that span from the inlet to the outlet. Flow entering these 'bypass channels' can travel through the heat sink without being pushed through any pin fin arrays, reducing the overall pressure drop but without contributing to the heat transfer. In all the designs, there are two large channels upstream and downstream of the hotspot, which guide the flow into and out of the dark gray features (tightly packed pin fin arrays) within the vicinity of the hotspot, similar to what is shown in Figure 4 (b). The benchmark straight microchannel (SMC) heat sink is also optimized for the same cost function and the resulting pareto optimality curve can be seen in Figure 7. Although both the channel width (w_c) and the fin thickness (t_f) are optimized, the optimal fin thickness is always at its lower bound of 150 µm dictated by the minimum allowed feature size. The pareto optimality curve for the benchmark is significant further from the origin compared to the curve for the topologically optimized designs, meaning that a lower thermal resistance (at a set pressure drop) or a lower pressure drop (at a set temperature limit) can universally be achieved by the topologically optimized designs. The performance improvement achieved by the topologically optimized designs is in part attributed to its ability to control the amount of flow routed to the hotspot versus background heat flux. In contrast, conventional designs such as the SMC heat sink consist of uniform geometries that are bound to have a uniform flow rate across the design space; the hotspot does not get priority even though has a significantly higher heat flux. Additionally,

the fractal-like designs created by topology optimization route the liquid to the effective heat transfer features through low-hydraulic-resistance pathways, reducing the overall pressure drop of the designs.
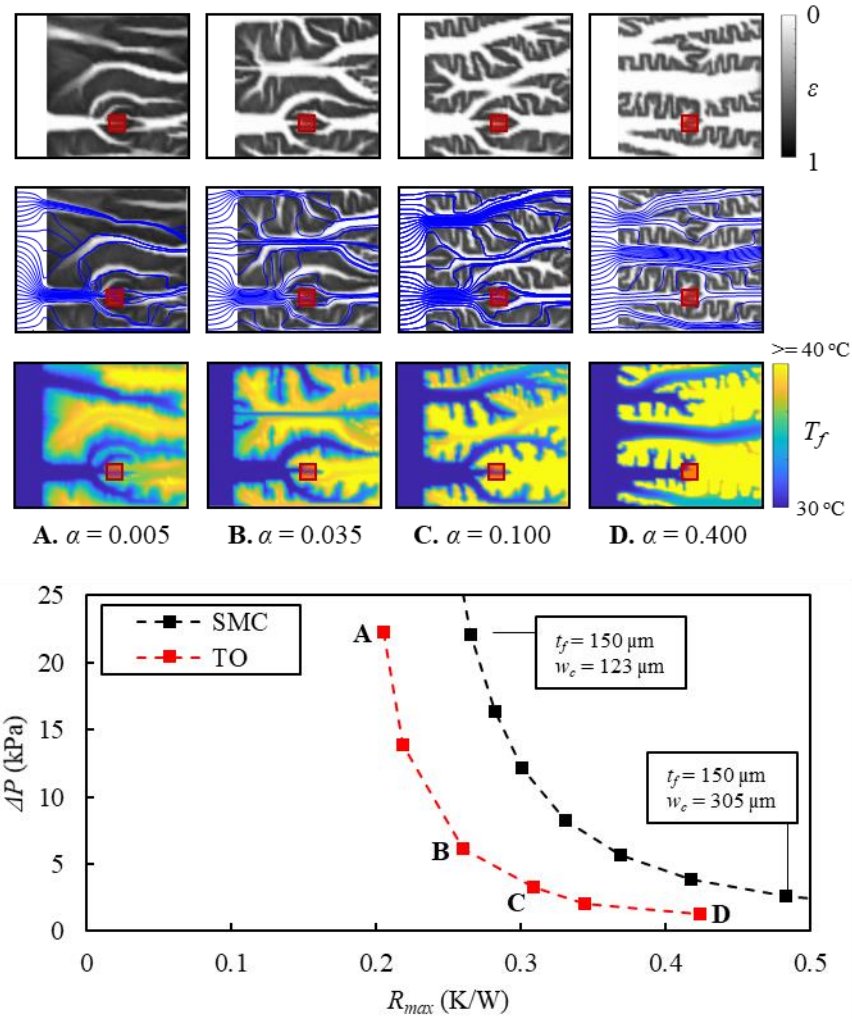

Figure 7: Pareto optimality curves for the topologically optimized designs and the optimized SMC designs generated by varying the weighting coefficient, α, in the objective function (Equation 1). Grayscale material distribution contour maps, streamlines, and coolant temperature maps of several selected topologically optimized designs along the curve at different weighting coefficients.

4. Conclusions

In conventional topology optimization, penalization approaches are used to achieve binary designs consisting of separate solid and liquid regions, also known as a restricted problem formulation. This work used a homogenization approach for topology optimization wherein the partial densities are represented physically as microstructures, allowing for sub-resolution features that would be otherwise require significantly more computational expensive (i.e., grid resolution) to resolve. A topology optimization method was developed that incorporates 3D-printing-friendly square pin fin microstructures to represent partial densities to design microchannel heat sinks. Height-averaged two-dimensional mass, momentum, and energy conservation equations were developed for flow through the porous medium with local thermal non-equilibrium between the solid and liquid phases. The resulting optimal topologies had fractal-like geometries where the liquid is transported through low-hydraulic-resistance pathways and selectively gets pushed through arrays of pin fins with tight spacing for effective heat transfer. The effects of the grid resolution and the initial design guess on the resulting topologies and performances were investigated. A multi-objective optimization approach was used to investigate the hydraulic and the thermal performance of the topologically optimized designs for a nonuniform heating boundary condition containing a local hotspot. The benchmark design, microchannel heat sink with straight channels, was also optimized for performance comparison. The following key conclusions were drawn:

- Although using higher resolution gives designs with much finer features, pressure drop and thermal resistance achieved by topologically optimized designs converge at a low resolution (40×40 grid cells for a 15×15 mm^2 design space). This is attributed to the relaxed problem formulation, where each cell is modeled using a physical microstructure, giving the optimizer the ability to use sub-resolution features within the design space. The smallest pin fin gap of 26.5 μm captured by the relaxed formulation using a 40×40 grid resolution in this paper would require a grid resolution of 567×567 if the restricted problem formulation is used.

- The appearance of the generated designs change significantly when the initial uniform material distribution provided to the optimizer is varied. However, the same characteristic flow features appear in all of the designs (viz., open manifold inlet/outlet channels feeding dense pin field arrays) and the difference in pressure drop and thermal resistance of the designs are minor.

- Topologically optimized designs achieve a lower thermal resistance (at a set pressure drop) or a lower pressure drop (at a set temperature limit) compared to the benchmark design, an SMC heat sink, when both designs are optimized for the same objective function. The thermal resistance is dominated by the temperature of the hotspot for the benchmark design where the flow is bound to uniformly distributed within the design space despite the nonuniform heating boundary conditions. Topology optimization is able to locally control the amount of coolant flow to the hotspot and background to achieve a lower thermal resistance.

References

[1] M. Wong, I. Owen, C. J. Sutcliffe, A. Puri, "Convective heat transfer and pressure losses across novel heat sinks fabricated by Selective Laser Melting," *International Journal of Heat and Mass Transfer,* vol. 52, no. 1–2, pp. 281-288, 2009.

[2] M. Fasano, L. Ventola, F. Calignano, D. Manfredi, E. P. Ambrosio, E. Chiavazzo, O. Asinari, "Passive heat transfer enhancement by 3D printed Pitot tube based heat sink," *International Communications in Heat and Mass Transfer,* vol. 74, pp. 36-39, 2016.

[3] P.-H. Tseng, K.-T Tsai, A.-L. Chen, C.-C. Wang, "Performance of novel liquid-cooled porous heat sink via 3-D laser additive manufacturing," *International Journal of Heat and Mass Transfer,* vol. 137, pp. 558-564, 2019.

[4] S. Ozguc, S. Pai, L. Pan, P. J. Geoghegan, J. A. Weibel, "Experimental Demonstration of an Additively Manufactured Vapor Chamber Heat Spreader," in *Intersociety Conference on Thermal and Thermomechanical Phenomena in Electronic Systems,* Las Vegas, NV, USA, 2019.

[5] I. L. Collins, J. A. Weibel, L. Pan, S. V. Garimella, "A permeable-membrane microchannel heat sink made by additive manufacturing," *International Journal of Heat and Mass Transfer,* vol. 131, pp. 1174-1183, 2019.

[6] S. Ozguc, L. Pan, J. A. Weibel, "Optimization of permeable membrane microchannel heat sink for additive manufacturing" (in review).

[7] H. A. Eschenauer, N. Olhoff, "Topology optimization of continuum structures, A review," *Applied Mechanics Reviews,* vol. 54, no. 4, pp. 331-390, 2001.

[8] J. D. Deaton, R. V. Grandhi, "A survey of structural and multidisciplinary continuum topology optimization: post 2000," *Structural and Multidisciplinary Optimization,* vol. 49, no. 1, pp. 1-38.

[9] A. A. Koga, E. C. C. Lopes, H. F. V. Nova, C. R. de Lima, E. C. N. Silva, "Development of heat sink device by using topology optimization," *International Journal of Heat and Mass Transfer,* vol. 64, pp. 759-772, 2013.

[10] M. Zhao, Y. Tian, M. Hu, F. Zhang, M. Yang, "Topology optimization of fins for energy storage tank with phase change material," *Numerical Heat Transfer,* vol 77, no. 3, pp. 284-301, 2020.

[11] S. Zeng, B. Kanargi, P. S. Lee, "Experimental and numerical investigation of a mini channel forced air heat sink designed by topology optimization," *International Journal of Heat and Mass Transfer,* vol. 121, pp. 663-679, 2018.

[12] E. M. Dede, "Multiphysics optimization, synthesis, and application of jet impingement target surfaces," in *Intersociety Conference on Thermal and Thermomechanical Phenomena in Electronic Systems,* Las Vegas, NV, USA, 2010.

[13] E. M. Dede, "Optimization and design of a multipass branching microchannel heat sink for electronics cooling," *Journal of Electronic Packaging,* vol. 134, no. 4, 2012.

[14] J. Alexandersen, O. Sigmund, N. Aage, "Large scale three-dimensional topology optimization of heat sinks cooled by natural convection," *International Journal of Heat and Mass Transfer,* vol. 100, pp. 876-891, 2016.

[15] S. B. Dilgen, C. B. Dilgen, D. R. Fuhrman, O. Sigmund, B. S. Lazarov, "Density based topology optimization of turbulent flow heat transfer systems," *Structural and Multidisciplinary Optimization,* vol. 57, no. 5, pp. 1905-1918.

[16] E. M. Dede, S. N. Joshi, F. Zhou, "Topology optimization, additive layer manufacturing, and experimental testing of an air-cooled heat sink," *Journal of Mechanical Design,* vol. 137, no. 11, pp. 111403, 2015.

[17] B. S. Lazarov, O. Sigmund, K. E. Meyer, J. Alexandersen, "Experimental validation of additively manufactured optimized shapes for passive cooling," *Applied Energy,* vol. 226, pp. 330-339, 2018.

[18] R. B. Haber, M. P. Bendsoe, "Problem formulation, solution procedures and geometric modeling: key issues in variable-topology optimization," in *Symposium on Multidisciplinary Analysis and Optimization,* St. Lous, MO, USA, 1998.

[19] M.P. Bendsoe, O. Sigmund, "Material interpolation schemes in topology optimization," *Archive of Applied Mechanics,* vol. 69, no. 9-10, pp. 635-645, 1999.

[20] B. Zhu, M. Skouras, D. Chen, W. Matusik, "Two-scale topology optimization with microstructures," *ACM Transactions on Graphics,* vol. 36, no. 5, p. 1-16, 2017.

[21] T. V. Oevelen, "Optimal heat sink design for liquid cooling of electronics," Ph.D. dissertation, Katholieke Universiteit Leuven, Leuven, Belgium, 2014.

[22] K. Svanberg, "The method of moving asymptotes—a new method for structural optimization," *International Journal for Numerical Methods in Engineering,* vol. 24, no. 2, pp. 359-373, 1987.

[23] O. Sigmund, "Morphology-based black and white filters for topology optimization," *Structural and Multidisciplinary Optimization,* vol. 33, no. 4-5, pp. 401-424, 2007.

[24] I. L. Collins, J. A. Weibel, L. Pan, S. V. Garimella, "Evaluation of additively manufactured microchannel heat sinks," *IEEE Transactions on Components, Packaging, and Manufacturing Technology,* vol. 9, no. 3, pp. 446-457, 2018.

[25] F. P. Incropera, D. P. DeWitt, T. L. Bergman, A. S. Lavine, "Fundamentals of Heat and Mass Transfer," *Wiley,* 2011.

[26] "Material Data Sheet – FlexLine, EOS Aluminum AlSi10Mg," https://www.eos.info.

[27] Krakat, G., "Cryostatic Bath Fluids, Aqueous Solutions, and Glycols," *VDI Heat Atlas,* pp. 435-457, 2010.

[28] S. Sarangi, K. K. Bodla, S. V. Garimella, J. Y. Murthy, "Manifold microchannel heat sink design using optimization under uncertainty," *International Journal of Heat and Mass Transfer,* vol. 69, pp, 92-105, 2014.